Transport properties of continuous-time quantum walks on Sierpinski fractals

Zoltán Darázs,[1,2,*] Anastasiia Anishchenko,[3,*] Tamás Kiss,[1] Alexander Blumen,[3] and Oliver Mülken[3]

[1] *WIGNER RCP, SZFKI, Konkoly-Thege Miklós út 29-33, H-1121 Budapest, Hungary*
[2] *Eötvös University, Pázmány Péter sétány 1/A, H-1117 Budapest, Hungary*
[3] *Physikalisches Institut, Universität Freiburg, Hermann-Herder-Straße 3, 79104 Freiburg, Germany*

(Dated: October 5, 2018)

We model quantum transport, described by continuous-time quantum walks (CTQW), on deterministic Sierpinski fractals, differentiating between Sierpinski gaskets and Sierpinski carpets, along with their dual structures. The transport efficiencies are defined in terms of the exact and the average return probabilities, as well as by the mean survival probability when absorbing traps are present. In the case of gaskets, localization can be identified already for small networks (generations). For carpets, our numerical results indicate a trend towards localization, but only for relatively large structures. The comparison of gaskets and carpets further implies that, distinct from the corresponding classical continuous-time random walk, the spectral dimension does not fully determine the evolution of the CTQW.

PACS numbers: 05.60.Gg, 05.60.Cd, 05.45.Df

I. INTRODUCTION

Networks are sets of connected nodes [1, 2], and their static and the dynamic properties are of much interest. Applications range from, say, polymer science [3], over traffic and power grid studies [4], up to social networks [5]. A special class of networks are deterministic fractals which as such can be built iteratively. We remark that for them sometimes analytic results can be obtained, see, e.g., Refs. [6–8].

Now, the classical dynamics of random walks (RW) over networks has been extensively investigated in the last decades [9, 10]. This effort has led to a very detailed understanding of the influence of the network's topology on RW. When the efficiency of transport is concerned, the question whether the RW is recurrent or transient boils down to determining the probability of the RW to return to its origin, which is also related to the Pólya number [11]. Moreover, the global properties of the RW can also be captured by introducing the local probability decay channels and calculating the averaged decay time of the excitation, known as the averaged mean first passage time (MFPT) [9, 12]. For simple undirected networks the transfer matrix of the continuous-time random walk (CTRW) is given by the connectivity matrix of the network [13]. Many networks show scaling behavior for the lower part of the spectrum of the connectivity matrix, with an exponent d_s which is called *spectral dimension* [14]. As it turns out, d_s determines many of the dynamical properties of the network, e.g., the return to the origin or the MFPT.

For the quantum mechanical aspects of transport on networks, we choose as a model the continuous-time quantum walk (CTQW), which is related to the classical CTRW [13]. In this way, the Hamiltonian is determined by the connectivity of the network. Therefore, by analyzing the connectivity matrix, we obtain results for both, CTRW and CTQW. While in recent years CTQW over several types of networks have been analyzed [13], there is no unambiguous classification according to, say, the spectral dimension. In many aspects, the quantum dynamics is much richer (i.e., more complex) than the classical CTRW counterpart, since it also involves the wave properties of the moving object. In several cases of tree-like networks, such as stars [15, 16] or dendrimers [17], it has been shown that the (average) quantum mechanical transport efficiency, defined by the return to the origin, is rather low compared to structures which are translationally invariant. Quantum walks are interesting models also from the point of view of quantum information processing [18]. Search via quantum walks on fractal graphs has been considered in Refs. [6, 19, 20].

A similar mathematical model arises for condensed matter systems, in which one considers a particle moving on an underlying fractal lattice (a Sierpinski gasket); here the solution of Schrödinger's equation has been studied within the tight-binding approximation [21, 22]. For several fractals considered, the dynamics has been shown to be subject to localization effects, similar to the classical waves in fractal waveguides [23]. From an experimental point of view, recent years have seen a growing number of possible implementations of CTQW, for example, using interference effects of light. Those experiments range from photonic waveguides [24] to fiber-loops [25].

In this paper we study quantum transport over fractal networks, namely over Sierpinski gaskets (SG) and their dual structures (DSC) as well as over Sierpinski carpets (SC) and their dual structures (DSC). In the case of the SG and of their duals we find clear signatures of localization around the initial starting node, indicating recurrent behavior. We seek to answer the question whether the spectral dimension d_s of the graph determines the transport properties for CTQW. Given the great experimental control over, say, coupling rates and decoherence, we believe that our results for fractal structures can also be experimentally realized, say, through photonic waveguides.

The paper is organized as follows, Sec. II gives an overview over the quantities we use to determine the performance of CTQW over networks. In Sec. III we outline the deterministic construction rules of the SG and SC and their dual transfor-

* These authors contributed equally to this work.

mations, along with their spectral properties. These systems are then analyzed in detail in Secs. IV-VII. We close with a summary of results in Sec. VIII.

II. METHODS

We model the quantum dynamics of an excitation over a given fractal network by CTQW and compare this to its classical counterpart, the CTRW, over the same network. A network is determined by a set of N nodes and a set of bonds. With each of the nodes we associate a state $|k\rangle$ corresponding to an excitation localized at node k. For both, CTQW and CTRW, the dynamics is determined by the network's connectivity, i.e., by its connectivity matrix $\mathbf{A}$. The off-diagonal elements of $\mathbf{A}$ are $A_{kj} = -1$ if the nodes k and j are connected by a single bond and are $A_{kj} = 0$ otherwise; the diagonal elements are $A_{kk} = f_k$, where f_k is the functionality of node k, i.e., the number of nodes connected to k through a single bond. The matrix $\mathbf{A}$ is real and symmetric and has only real and non-negative eigenvalues. For networks without disjoint parts all eigenvalues are positive except one, $E_{min} = 0$.

Now, we take for CTRW the transfer matrix $\mathbf{T} = -\mathbf{A}$ and for CTQW the Hamiltonian $\mathbf{H} = \mathbf{A}$ (i.e. in the following we set $\hbar = 1$ and normalize the transfer capacity of each bond to unity), see also [13, 26], such that the transition probabilities read $p_{k,j}(t) = \langle k| \exp(\mathbf{T}t)|j\rangle$ and $\pi_{k,j}(t) = |\langle k| \exp(-i\mathbf{H}t)|j\rangle|^2$, respectively. By diagonalizing $\mathbf{A}$ we obtain the eigenvalues E_n and the eigenstates $|\Phi_n\rangle$ (with $n = 1, \ldots, N$) of $\mathbf{A}$, resulting in

$$p_{k,j}(t) = \sum_{n=1}^{N} \exp(-E_n t)\langle k|\Phi_n\rangle\langle\Phi_n|j\rangle \tag{1}$$

for CTRW and

$$\pi_{k,j}(t) = \left|\sum_{n=1}^{N} \exp(-iE_n t)\langle k|\Phi_n\rangle\langle\Phi_n|j\rangle\right|^2 \tag{2}$$

for CTQW. In principle all quantities of interest can be calculated on the basis of the transition probabilities. In order to quantify the efficiency of the transport, we will focus on three quantities: the exact return probability and the related Pólya number, the average return probability, and the mean survival probability.

A. Pólya number

The so-called Pólya number allows to assess the *local* transport properties. In classical systems, the definition of the recurrence is straightforward: it characterizes the event that the walker returns to its initial position. For quantum walks one can imagine different definitions depending on the envisaged measurement procedure [27–33].

Ref. [34] suggests a possible quantum definition for the Pólya number, which is directly related to the return probability to the initial node ($|\psi(0)\rangle = |1\rangle$):

$$\pi_{1,1}(t) = |\langle 1| \exp(-i\mathbf{H}t)\,|1\rangle|^2 \ . \tag{3}$$

The formal definition of the Pólya number reads

$$\mathcal{P} = 1 - \prod_{i=1}^{\infty}[1 - \pi_{1,1}(t_i)]\,, \tag{4}$$

where the set $\{t_i, i = 1, \ldots \infty\}$ is an infinite time series which can be chosen regularly or be determined by some random process. It can be shown that its value depends on the convergence speed of $\pi_{1,1}(t)$ to zero: if $\pi_{1,1}(t)$ converges faster than t^{-1} then the CTQW is transient, otherwise it is recurrent [34].

For a finite network of N sites the probability that we find the walker at the origin can be written as a finite sum of cosine functions,

$$\begin{aligned}\pi_{1,1}(t) &= \left|\sum_{n=1}^{N}\langle 1|e^{-iE_n t}|\Phi_n\rangle\langle\Phi_n|1\rangle\right|^2 \\ &= \sum_{n,m=1}^{N} |\langle 1|\Phi_n\rangle|^2|\langle 1|\Phi_m\rangle|^2 \cos\left[(E_m - E_n)t\right] \ . \end{aligned} \tag{5}$$

A finite sum of cosine functions cannot be a decaying function of time and thus for any finite system the Pólya number equals one, meaning that the walk is recurrent. On the other hand, in an infinite network ($N \to \infty$), $\pi_{1,1}(t)$ might tend to zero in the $t \to \infty$ limit. If the return probability has the asymptotic form $\pi_{1,1}(t) \sim f(t) \cdot t^{-\delta}$ where $f(t)$ is a periodic or an almost periodic analytical function, then, with regular and Poissonian sampling, the walk is recurrent if $\delta \leq 1$, and it is transient if the envelope decays faster ($\delta > 1$) [34]. For CTRW on the fractals considered in the following, the decay of the probability $p_{1,1}(t)$ is slower than t^{-1}, which can be seen from the fact that on a fractal $p_{1,1}(t)$ scales as $t^{-d_s/2}$ and the fractals considered in this paper have spectral dimension $d_s < 2$ [35, 36].

B. Average return probability

As a *global* efficiency measure, the average return probability is defined as the probability to remain or return to the initial node j, averaged over all nodes:

$$\overline{p}(t) \equiv \frac{1}{N}\sum_{j=1}^{N} p_{j,j}(t) \tag{6}$$

$$\text{and} \qquad \overline{\pi}(t) \equiv \frac{1}{N}\sum_{j=1}^{N} \pi_{j,j}(t). \tag{7}$$

While $\overline{p}(t)$ only depends on the eigenvalues, $\overline{\pi}(t)$ also depends on the eigenstates. However, by using the Cauchy-Schwarz inequality a lower bound, independent of the eigenstates, has been introduced in [15]:

$$\overline{\pi}(t) = \frac{1}{N}\sum_{j=1}^{N} \pi_{j,j}(t) \geq \left|\frac{1}{N}\sum_{j=1}^{N} \alpha_{j,j}(t)\right|^2 \equiv \left|\,\overline{\alpha}(t)\right|^2. \tag{8}$$

In Eq. (8) $\alpha_{j,j}(t) = \langle j| \exp(-i\mathbf{H}t)|j\rangle$ is the transition amplitude between two nodes. In the following we will compare $\overline{p}(t)$ with $\left|\overline{\alpha}(t)\right|^2$ and express both quantities in terms of the (discrete) density of states (DOS)

$$\tilde{\rho}(E) = \frac{1}{N}\sum_{n=1}^{N} \delta(E - E_n)\,. \tag{9}$$

Here $\delta(E - E_n)$ is the Dirac delta-function. Integrating $\tilde{\rho}(E)$ in a very small neighborhood of an eigenvalue, say, E_m, gives

$$\lim_{\varepsilon\to 0^+} \int_{E_m-\varepsilon}^{E_m+\varepsilon} \tilde{\rho}(E)\,\mathrm{d}E = D(E_m)/N \equiv \rho(E_m)\,. \tag{10}$$

where $D(E_m)$ is the degeneracy of E_m and we introduced $\rho(E)$. This yields

$$\begin{aligned}\overline{p}(t) &= \sum_{\{E_m\}} \rho(E_m)\exp(-E_m t) \\ &= \int_{-\infty}^{\infty} \tilde{\rho}(E)\exp(-Et)\,\mathrm{d}E \end{aligned} \tag{11}$$

and

$$\begin{aligned}\left|\overline{\alpha}(t)\right|^2 &= \Big|\sum_{\{E_m\}} \rho(E_m)\exp(-iE_m t)\Big|^2 \\ &= \Big|\int_{-\infty}^{\infty} \tilde{\rho}(E)\exp(-iEt)\,\mathrm{d}E\,\Big|^2, \end{aligned} \tag{12}$$

where the sums run over the set $\{E_m\}$ of *distinct* eigenvalues.

Now, if both $\overline{p}(t)$ and $\left|\overline{\alpha}(t)\right|^2$ decay very quickly in time, the average probability to find the excitation at any node but the initial node increases quickly. Then we call the transport over the network efficient, because (on average) the excitation will efficiently explore parts of the network away from the initial node. In contrast, if these quantities decay very slowly, we regard the transport as being inefficient.

For CTRW and not too short times, $\overline{p}(t)$ is dominated by the small eigenvalues. For fractals, the DOS typically scales with the so-called spectral dimension d_s [14], i.e., $\tilde{\rho}(E) \sim E^{d_s/2-1}$. Then, one finds in an intermediate time range, before the equilibrium value is reached, that $\overline{p}(t) \sim t^{-d_s/2}$. However, for CTQW such a simple analysis does not hold due to the coherent evolution. Instead, highly degenerate eigenvalues dominate $\left|\overline{\alpha}(t)\right|^2$, see Ref. [21, 37]. In the case that one has a single highly degenerate eigenvalue E_m, the lower bound of the average return probability can be approximated by [16]

$$\begin{aligned}|\bar{\alpha}(t)|^2 \approx \tilde{\rho}^2(E_m) + \tilde{\rho}(E_m) \lim_{\varepsilon\to 0^+} \Bigg[\int_{-\infty}^{E_m-\varepsilon} \tilde{\rho}(E) \\ \cos\big[(E-E_m)t\big]\mathrm{d}E + \int_{E_m+\varepsilon}^{\infty} \tilde{\rho}(E)\cos\big[(E-E_m)t\big]\mathrm{d}E\Bigg]. \end{aligned} \tag{13}$$

If there is at least one eigenvalue for which $\tilde{\rho}(E_m)$ is $\mathcal{O}(1)$, then the average transition amplitude does not tend to zero. Then the long time average $\overline{\chi}_{lb}$ of the transition probability also allows to quantify the global performance of CTQW through [16]

$$\overline{\chi}_{lb} = \lim_{T\to\infty}\frac{1}{T}\int_0^T |\bar{\alpha}(t)|^2\,\mathrm{d}t = \sum_{\{E_m\}} \left[\tilde{\rho}(E_m)\right]^2 . \tag{14}$$

C. Mean survival probability

In order to corroborate our findings for the average return probabilities, we define another (global) transport efficiency measure which is based on the mean survival probability, see also [38] for CTQWs and [39] for discrete time quantum walks. Here, the original network is augmented by local decay channels which act as traps for the walker. These traps are localized at a set $\mathcal{M}$ of nodes m of the original network. For this the total number of nodes of the system is not changed, but the transfer matrix $\mathbf{T}$ as well as the Hamiltonian $\mathbf{H}$ get augmented by additional terms, such that the new (effective) matrices read $\mathbf{T}_{\text{eff}} \equiv \mathbf{T} - \mathbf{\Gamma}$ and $\mathbf{H}_{\text{eff}} \equiv \mathbf{H} - i\mathbf{\Gamma}$, respectively, where the trapping matrix is diagonal, namely $\mathbf{\Gamma} = \Gamma\sum_{m\in\mathcal{M}} |m\rangle\langle m|$ with a trapping rate Γ which we set equal for all traps. We note that such an effective Hamiltonian can be obtained within the framework of quantum master equations of Lindblad type, where the network is only coupled to the environment at the trap nodes, see Ref. [40]. For CTRW, such traps will still lead to a real symmetric transfer matrix, but now with only positive eigenvalues [9]. For CTQW, the new Hamiltonian $\mathbf{H}_{\text{eff}}$ becomes non-Hermitian. Such Hamiltonians can have complex eigenvalues $E_n = \epsilon_n - i\gamma_n$ with a real part ϵ_n and an imaginary part γ_n. As has been shown in [38], by averaging the transition probabilities over all possible initial and final nodes one obtains the mean survival probability for CTQW as a function solely of the γ_n,

$$\Pi(t) \equiv \frac{1}{N}\sum_{j,k=1}^{N} \pi_{k,j}(t) = \frac{1}{N}\sum_{n=1}^{N} \exp(-2\gamma_n t)\,. \tag{15}$$

Note the slightly different definition of $\Pi(t)$ compared to the one in Ref. [38]. Here we do not exclude the trap nodes from the sum, thus Eq. (15) becomes exact. For CTRW a similar approach with the new transfer matrix $\mathbf{T}_{\text{eff}}$ yields [41]

$$P(t) \equiv \frac{1}{N}\sum_{j,k=1}^{N} p_{k,j}(t) = \frac{1}{N}\sum_{n=1}^{N} \exp(-\lambda_n t)\Big|\sum_{j=1}^{N}\langle j|\Psi_n\rangle\Big|^2, \tag{16}$$

where λ_n and $|\Psi_n\rangle$ are the eigenvalues and eigenstates of $\mathbf{T}_{\text{eff}}$, respectively. Thus, $P(t)$ will eventually decrease to zero and the asymptotical behavior will be dominated by the smallest eigenvalue. Now, if $\Pi(t)$ and $P(t)$ decrease quickly we also call the transport efficient (on average) because then an initial excitation will reach the trap rather quickly.

For CTQW one can relate the γ_n to the eigenstates of the original Hamiltonian $\mathbf{H}$ within a (non-degenerate) perturbative treatment, $\gamma_n = \Gamma\sum_{m\in\mathcal{M}} \left|\langle m|\Phi_n\rangle\right|^2$ [13]. Thus, the

imaginary parts γ_n are determined by the overlap of the eigenstates $|\Phi_n\rangle$ of $\mathbf{H}$ with the locations of the traps. This implies that for localized eigenstates this overlap can be zero, such that for some n the imaginary parts vanish, $\gamma_n = 0$. This yields a mean survival probability which does not decay to zero but which reaches the asymptotic value

$$\Pi_\infty \equiv \lim_{t\to\infty} \Pi(t) = \frac{N_0}{N}\,, \tag{17}$$

where N_0 is the number of eigenstates for which the γ_n vanish. For the SG it has been shown that such eigenstates exist, which in fact gives rise to localization effects [21].

We have now defined the asymptotic quantity Π_∞ which allows us to assess the transport properties of CTQW by calculating the probability that the walker will stay forever in the network.

III. THE SYSTEMS UNDER STUDY

We now discuss the systems under study and their topological properties. We consider two groups of Sierpinski fractals, namely, gaskets and carpets, along with their dual transformations. These fractals are built in an iterative manner: In order to construct the SG, one starts from a triangle of three nodes. In the next step two additional triangles are attached to the corner nodes by merging them, so that they form a bigger self-similar triangle. The procedure is then iterated, see Fig. 1(a) for a gasket at generation $g = 3$. A similar idea is used for creating SC, where instead of triangles the central building blocks are squares, see also Fig. 1(c). At generation g the total number of nodes of the SG is $N_{\rm SG} = (3^g + 3)/2$ and of the SC is $N_{\rm SC} = \frac{11}{70}\cdot 8^g + \frac{8}{15}\cdot 3^g + \frac{8}{7}$, so that at the same (large) g the carpet has much more nodes than the gasket.

The dual networks of the Sierpinski fractals are easily obtained by the following procedure: In the original structure one replaces each of the smallest building blocks (triangles for gaskets and squares for carpets) by a node and connects then the nodes which belong to building blocks sharing a node (for carpets we only allow connections in the horizontal and in the vertical direction but not diagonally), see also Figs. 1(b) and 1(d), which illustrate the procedure by also showing the underlying lattices of the SG and SC, respectively. The number of nodes of the DSG of generation g is $N = 3^g$ and of the DSC of generation g is $N = 8^g$.

Based on real space renormalization arguments, one can show that a structure and its dual have the same fractal d_f and spectral d_s dimensions. For the SG and the DSG, the corresponding values are $d_f = \ln(3)/\ln(2) \approx 1.5849\ldots$ and $d_s = 2\ln(3)/\ln(5) \approx 1.3652\ldots$, see Ref. [6]. For the SC and the DSC, one has $d_f = \ln(8)/\ln(3) \approx 1.8928\ldots$ and $d_s \approx 1.805$ [36].

For our calculations of the average return probabilities we assume that every single node of the network can be the origin of the walk with the same probability and that the average runs over all sites $j = 1, \ldots, N$. For the individual return probability $\pi_{j,j}(t)$ we use the outer corner node 1 as initial node. As for the mean survival probabilities, we will distinguish between two situations: (1) when there are three (four) trap nodes at the outer corners of the gasket (carpet), see the red diamonds in Fig 1, and (2) when the three (four) trap nodes are placed at the corners of the largest empty inner triangle (square) of the gasket (carpet), see the red squares in Fig. 1. Since the quickest decay of $\Pi(t)$ for the linear networks studied in Ref. [38] is obtained when the trapping strength Γ is of the same order of magnitude as the coupling between the nodes, we choose $\Gamma = 1$ in all calculations involving traps.

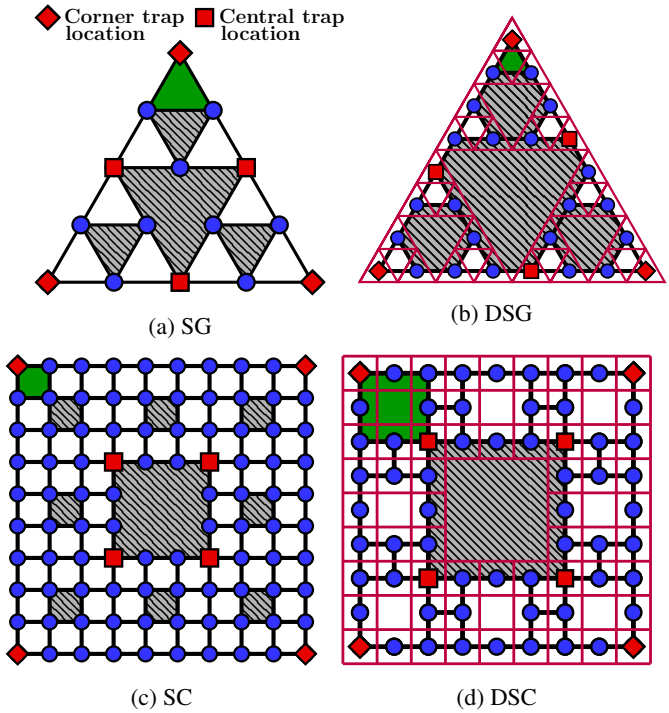

(a) SG (b) DSG

(c) SC (d) DSC

FIG. 1: (Color online) The graphs under study. The graphs are at third generation ($g = 3$), except the DSC for which $g = 2$. We denoted the $g = 1$ graphs with green, and the holes with a gray (striped) background. Traps are put either at the positions indicated by the small diamonds or at the positions indicated by the small squares.

Let us first consider systems without traps. Since the eigenvalue distributions are crucial for determining the global efficiency measures, we start by considering the differences between our four fractal structures. In Fig. 2 we plot for several structures the normalized cumulative eigenvalue counting function

$$\mathcal{N}(x) = \frac{1}{N}\sum_{n=1}^{N} \theta(x - \frac{E_n}{E_{max}}), \tag{18}$$

where $\theta(x)$ is the Heaviside-function. Now, $E_{min} = 0$ is the smallest and E_{max} the largest eigenvalue, hence, the range of x is $[0, 1]$.

Already here we can exemplify the role of highly degenerate eigenvalues. For large N the eigenvalue counting function

for an $N \times N$ square lattice is a quite smooth function, which for $N \to \infty$ we plot as a reference in Fig. 2.

Also the SC for $g = 6$ leads to a quite smooth form for $\mathcal{N}(x)$. However, $\mathcal{N}(x)$ for the DSC of $g = 5$ displays marked steps, but its overall shape is close to the one for the SC. For the SG for $g = 9$ and its dual, the DSG for $g = 9$, $\mathcal{N}(x)$ has sharp discontinuities, which reflect the presence of many highly degenerate eigenvalues. Already at this point we see a clear distinction between gaskets and carpets: at similar g the carpets do not have eigenvalues of such high degeneracy as the gaskets.

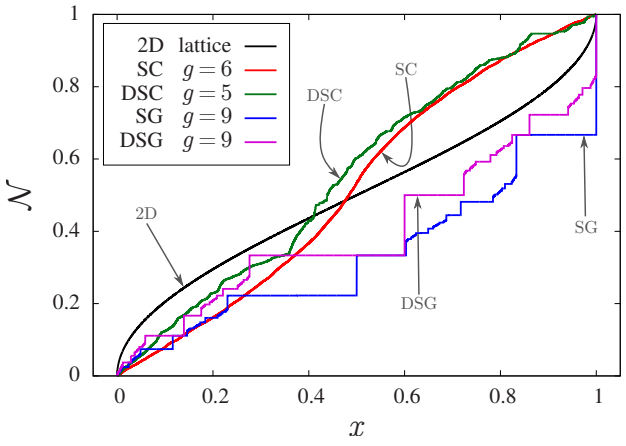

FIG. 2: (Color online) The eigenvalue counting function $\mathcal{N}(x)$, Eq. (18), for several systems under study, compared to the simplest case of an infinite discrete square lattice, see text for details.

IV. DUAL SIERPINSKI GASKET

We start by considering the DSG, see also Fig. 1(b). As the SG, the DSG is a deterministic fractal, iteratively built up generation by generation. CTQW on DSG of different generations have been studied by us in Ref. [6]. We will recapitulate the major results, since we will use the DSG as a reference for our new results presented below. In fact, DSG is special, in that its eigenvalues, and hence its DOS can be determined iteratively, in a simple way. This does not hold for the other fractals considered here.

For DSG the results for the CTRW and CTQW return probabilities $p_{1,1}(t)$ and $\pi_{1,1}(t)$, along with the CTQW lower bound $\left|\overline{\alpha}(t)\right|^2$ of $\overline{\pi}(t)$ (see Eqs. (1), (2), and (8), respectively) have been already presented in Ref. [6]. There it has been verified that for the classical average return probability, the decay to the equipartition value is determined solely by d_s [42], having namely $\overline{p}(t) \sim t^{-d_s/2}$. It follows that the classical walk on DSG is recurrent and that the Pólya number equals unity. As we will show below for all the fractal types considered here, such a quite simple law does not hold for CTQW.

Turning now to the quantum case and evaluating the lower bound $\left|\overline{\alpha}(t)\right|^2$ of $\overline{\pi}(t)$ of the quantum average return probability $\overline{\pi}(t)$, see Eq. (8), it has been found in [6] that its envelope does not show a strong dependence on the size of the DSG. Since the two eigenvalues 3 and 5 make up for about $1/3$ of all eigenvalues, they control most of the behavior of $\overline{\pi}(t)$. Then $\rho(3)$ and $\rho(5)$ are known in closed form,

$$\rho(3) = \frac{1}{2 \cdot 3^g} \left(3^{g-1} + 3\right) \tag{19}$$

and

$$\rho(5) = \frac{1}{2 \cdot 3^g} \left(3^{g-1} - 1\right) . \tag{20}$$

In particular, also the long time average $\overline{\chi}_{lb}$ can be calculated exactly, based on Eq. (14)

$$\overline{\chi}_{lb} = \frac{1}{3^{2g}} \left[3^g \left(1 + \frac{3^g}{14}\right) + \frac{10}{7} 2^g - \frac{3}{2}\right] , \tag{21}$$

which for large g is much larger than the equipartition value 3^{-g}. The limit $g \to \infty$ yields

$$\lim_{g \to \infty} \overline{\chi}_{lb} = 1/14 \approx 0.0714 . \tag{22}$$

For both highly degenerate eigenvalues, TABLE I shows $\rho(3)$ and $\rho(5)$, Eq. (10), for successive generations g from 2 to 8, calculated according to Eqs. (19) and (20). Also the exact value of $\overline{\chi}_{lb}$, see Eq. (21), is shown. Both $\rho(3)$ and $\rho(5)$ tend to the exact limiting value $1/6$, see Eqs. (19) and (20), rather fast, which, together with Eq. (13), means that the transport is quite inefficient.

Now, we calculate for the DSG $\Pi_\infty^{(1)}$ and $\Pi_\infty^{(2)}$ using Eq. (17). In order to do this, we numerically determine the eigenvalues of the non-Hermitian $\mathbf{H}_{\text{eff}}$, paying particular attention to their imaginary parts γ. We do this using the MATLAB / GNU Octave eig() function, and in order to be more precise, we employed the LAPACK zgeev() function in our Fortran code with quadruple precision. Despite these efforts, the procedure may not be exact, however. First, we cannot exclude the existence of very small, but nonzero imaginary parts which are smaller than 10^{-31} and are set to zero. Second, numerical errors may induce small imaginary contributions where there should be none. Thus, the values in our table for Π_∞ may not be as exact as their form seems to imply.

Counting all the eigenvalues with vanishing imaginary part we then obtain N_0. From it we readily evaluate $\Pi_\infty^{(1)}$ and $\Pi_\infty^{(2)}$, see Eq. (17). In the next sections, the same procedure will be employed for the other fractals studied. The analysis of the data of TABLE II shows that $\Pi_\infty^{(1)}$ and $\Pi_\infty^{(2)}$ increase with increasing g, which means that N_0 increases faster than N. Already for $g = 7$, corresponding to a network of $N = 2187$ nodes, the probabilities $\Pi_\infty^{(1)}$ and $\Pi_\infty^{(2)}$ that the walker survives within the network are close to 0.855 and to 0.826, respectively. We note that the values of $\Pi_\infty^{(2)}$ are somewhat below the ones for $\Pi_\infty^{(1)}$, implying that here traps on the periphery act somewhat less efficiently than centrally located traps.

g	$\rho(3)$	$\rho(5)$	$\overline{\chi}_{lb}$
2	$1/3 \approx 0.3333$	$1/9 \approx 0.1111$	0.2346
3	$2/9 \approx 0.2222$	$4/27 \approx 0.1481$	0.1221
4	$5/27 \approx 0.1852$	$13/81 \approx 0.1605$	0.0870
5	$14/81 \approx 0.1728$	$40/243 \approx 0.1646$	0.0763
6	$41/243 \approx 0.1687$	$121/729 \approx 0.1660$	0.0730
7	$122/729 \approx 0.1674$	$364/2187 \approx 0.1664$	0.0719
8	$365/2187 \approx 0.1669$	$1093/6561 \approx 0.1666$	0.0716

TABLE I: The $\rho(E)$ for the eigenvalues $E = 3$ and $E = 5$ and the long time average $\overline{\chi}_{lb}$ for different generations of the DSG.

g	$\Pi_\infty^{(1)} = N_0^{(1)}/N$	$\Pi_\infty^{(2)} = N_0^{(2)}/N$
2	$1\,/\,9 \approx 0.111$	0
3	$9\,/\,27 \approx 0.333$	$6\,/\,27 \approx 0.222$
4	$43\,/\,81 \approx 0.531$	$36\,/\,81 \approx 0.444$
5	$165\,/\,243 \approx 0.679$	$150\,/\,243 \approx 0.617$
6	$571\,/\,729 \approx 0.783$	$540\,/\,729 \approx 0.741$
7	$1869\,/\,2187 \approx 0.855$	$1806\,/\,2187 \approx 0.826$

TABLE II: The asymptotic limit Π_∞ of $\Pi(t)$ for DSG of generations $g = 2, 3 \ldots, 7$; case (1): the traps are placed on the corner nodes, diamonds in Fig. 1(b); case (2): the traps are placed on the central nodes, squares in Fig. 1(b), see text for details.

V. SIERPINSKI GASKET

While the DSG allows for partly analytical results, we have to resort to numerical calculations for the other structures considered in this paper. We proceed our investigation with the SG. In analogy to our study on DSG, we start with the CTRW and CTQW return probabilities as well as with the lower bound for the CTQW decay. These quantities involve the eigenvalues and (depending on the functions considered) sometimes also the eigenstates of the Hermitian operators $\mathbf{T}$ and $\mathbf{H}$, see Eqs. (1)-(2). Unlike the DSG case, for SG general recursive expressions for the eigenvalues of $\mathbf{T}$ and $\mathbf{H}$ are not known. Therefore, we calculate both the eigenvalues and the eigenfunctions numerically. For this, we again use the MATLAB / GNU Octave eig() and eigs() functions. For large generations, we calculate only the spectrum in order to evaluate $|\overline{\alpha}(t)|^2$ and the $D(E_m)$ degeneracy of the eigenvalue E_m using the filtered Lanczos algorithm in C++ [43], and the MATLAB / GNU Octave eigs() function.

Figure 3 shows the classical $p_{1,1}(t)$ and the quantum mechanical $\pi_{1,1}(t)$ return probabilities to the initially excited node $j = 1$ for a SG with $g = 7$. The red dashed line in Fig. 3 gives the CTRW return probability $p_{1,1}(t)$. While the algebraic decay of $p_{1,1}(t) \sim t^{-d_s/2}$ holds asymptotically only for an infinite fractal, one can still recognize this scaling behavior in an intermediate time domain in Fig. 3, before $p_{1,1}(t)$ saturates to the equipartition value $1/N$ at long times. Figure 3 also shows the exact quantum return probability $\pi_{1,1}(t)$ (green solid line). After an initial decay to a local minimum, the return probability starts to oscillate around its long time average. In the inset of Fig. 3 we present the quantum mechanical lower bound $\left|\overline{\alpha}(t)\right|^2$ of the quantum average return probability $\overline{\pi}(t)$; $\left|\overline{\alpha}(t)\right|^2$ does not decay eventually, but shows strong oscillations with a long time average $\overline{\chi}_{lb}$ (dashed black line in Fig. 3) which is orders of magnitude larger than $1/N$. Now, in contrast to CTRW, there is no apparent relation between the spectral dimension and the return probability.

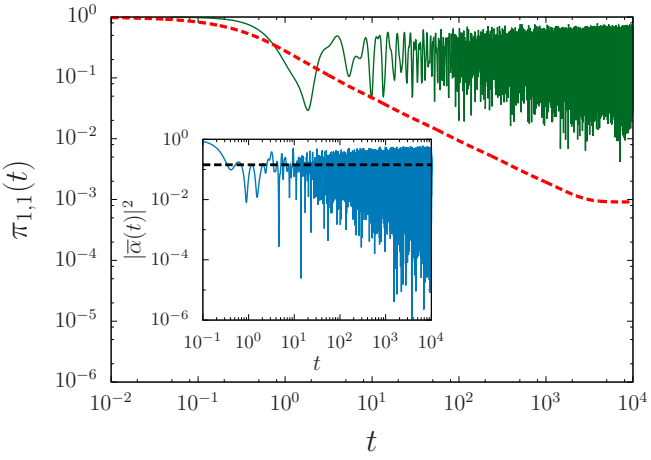

FIG. 3: (Color online) Quantum return probability $\pi_{1,1}(t)$ to the corner node $j = 1$ (green solid line) along with its classical analogue (red dashed line) for the SG of $g = 7$. Inset: CTQW lower bound $\left|\overline{\alpha}(t)\right|^2$ of $\overline{\pi}(t)$ on the SG at $g = 7$ (blue solid line) and $\overline{\chi}_{lb}$, the long time value (black dashed line).

The spectrum of the Hamiltonian already reveals whether CTQW shows localization. For different generations of the SG, we calculate, based on Eq. (10), the $\rho(E)$ of the highly degenerate eigenvalue 6, $\rho(6)$ and, based on the r.h.s. of Eq. (14), the long-time average $\overline{\chi}_{lb}$. The data are presented in TABLE III. As in the case of the DSG, also for SG the $\rho(6)$ seem to converge with increasing g to the finite limiting value $1/3$. As before, such a relatively large nonvanishing value lets us infer that the transport is not very efficient.

We now turn to CTQW on SG in the presence of traps, process which introduces non-Hermitian operators. In TABLE

g	$\rho(6)$	$\overline{\chi}_{lb}$
2	0	0.2778
3	3 / 15 = 0.2	0.1378
4	12 / 42 ≈ 0.2857	0.1179
5	39 / 123 ≈ 0.3171	0.1296
6	120 / 366 ≈ 0.3279	0.1374
7	363 / 1095 ≈ 0.3315	0.1408
8	1092 / 3282 ≈ 0.3327	0.1421
9	3279 / 9843 ≈ 0.3331	0.1426

TABLE III: The $\rho(E)$ for the eigenvalue $E = 6$ and the long time average $\overline{\chi}_{lb}$ for different generations of the SG.

g	$\Pi_\infty^{(1)} = N_0^{(1)}/N$	$\Pi_\infty^{(2)} = N_0^{(2)}/N$
2	0	0
3	4 / 15 ≈ 0.27	1 / 15 ≈ 0.067
4	21 / 42 = 0.5	15 / 42 ≈ 0.357
5	82 / 123 ≈ 0.67	70 / 123 ≈ 0.569
6	285 / 366 ≈ 0.78	261 / 366 ≈ 0.713
7	934 / 1095 ≈ 0.85	886 / 1095 ≈ 0.809

TABLE IV: The asymptotic limit Π_∞ of $\Pi(t)$ for SG of generations $g = 2, 3 \ldots, 7$; case (1): the traps are placed on the corner nodes, diamonds in Fig. 1(a); case (2): the traps are placed on the central nodes, squares in Fig. 1(a), see text for details.

IV, we show $\Pi_\infty^{(1)}$ and $\Pi_\infty^{(2)}$ for two situations, namely when the traps are placed on the corners and when the traps are placed in the center of the structure, see Fig. 1(a) for details. TABLE IV suggests that the situation is quite similar to the one for the DSG: the higher g the less it is probable that the excitation will be absorbed even after a very long time, see the increase in the Π_∞-values. However, the amount of excitation which stays localized in the network is higher in case (1) than in case (2), since $\Pi_\infty^{(1)} > \Pi_\infty^{(2)}$.

VI. DUAL SIERPINSKI CARPET

We continue our analysis by considering the SC and the DSC. We start with the DSC, the spectrum and harmonic functions of which have been considered recently [44, 45].

Figure 4 presents the lower bound $|\overline{\alpha}(t)|^2$ of the quantum $\overline{\pi}(t)$ for $g = 5$, see Eq. (8). The inset of Figure 4 depicts the classical return probability $p_{1,1}(t)$ given by Eq. (1). We note that at intermediate times $p_{1,1}(t)$ shows an algebraic decay with slope $d_s/2$. Furthermore, $|\overline{\alpha}(t)|^2$ displays at short to intermediate time a decay of the maxima, while at longer times it slowly approaches $\overline{\chi}_{lb}$, given in Fig. 4 through a dotted line around which it oscillates. Given that for DSC $\overline{\chi}_{lb}$ is much smaller than the corresponding $\overline{\chi}_{lb}$ for SG and for DSG, we infer that localization effects are smaller for DSC than for SG and for DSG.

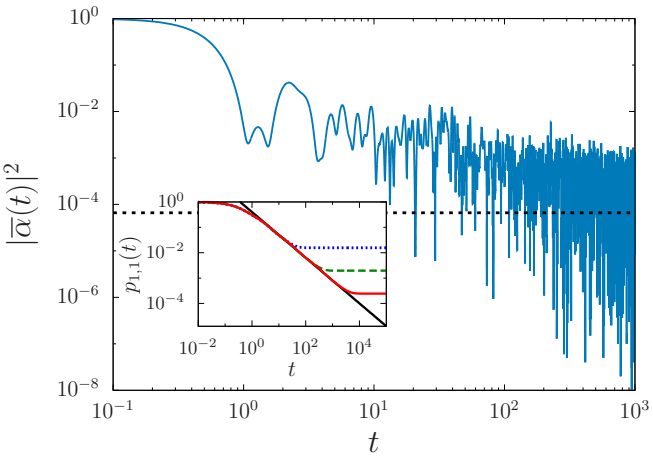

FIG. 4: (Color online) The average return amplitude $|\overline{\alpha}(t)|^2$ on the DSC of $g = 5$ (blue solid line) and the long time average (black dotted line). Inset: classical return probability $p_{1,1}(t)$ for DSC of $g = 2, 3$, and 4 (dotted blue, dashed green, solid red line, respectively) as well as the fitted decay (solid straight black line), $0.4 \cdot t^{-1.8/2}$.

g	$\rho(3)$	$\overline{\chi}_{lb}$
2	2 / 64 ≈ 3.13×10^{-2}	2.44×10^{-2}
3	4 / 512 ≈ 7.81×10^{-3}	2.98×10^{-3}
4	20 / 4096 ≈ 4.88×10^{-3}	3.89×10^{-4}
5	148 / 32768 ≈ 4.52×10^{-3}	6.60×10^{-5}
6	1172 / 262144 ≈ 4.47×10^{-3}	–

TABLE V: The $\rho(3)$ for the eigenvalue $E = 3$ and the long time average $\overline{\chi}_{lb}$ for different generations of the DSC.

g	$\Pi_\infty^{(1)} = N_0^{(1)}/N$	$\Pi_\infty^{(2)} = N_0^{(2)}/N$
2	15 / 64 ≈ 0.234	14 / 64 ≈ 0.219
3	126 / 512 ≈ 0.246	126 / 512 ≈ 0.246
4	1030 / 4096 ≈ 0.251	1030 / 4096 ≈ 0.251

TABLE VI: The asymptotic limit Π_∞ of $\Pi(t)$ for DSC of generations $g = 2, 3$, and 4; case (1): the traps are placed on the corner nodes, diamonds in Fig. 1(d); case (2): the traps are placed on the central nodes, squares in Fig. 1(d), see text for details.

However, from the above results we cannot deduce whether the walk is recurrent or not. Therefore, for DSC we again consider the spectrum of $\mathbf{T}$ and $\mathbf{H}$ and calculate, based on Eq. (10), $\rho(E)$ for the most highly degenerate eigenvalue, see TABLE V. Clearly, our calculations are limited by computational power and for the DSC we could not obtain results for g larger than 6; for $g = 6$ there are already $N = 262144$ nodes

in the network. It seems as if for very large g the $\rho(3)$ series will converge to a value somewhat above 4.4×10^{-3}. This finite limit again seems to indicate that there is localization in the system, so that CTQW may be recurrent in general.

Now, let us consider the CTQW trapping process for the DSC. TABLE VI presents Π_∞ for two different trap placements on DSC of $g = 2, 3$, and 4, as shown in Fig. 1(d). Our calculations of the mean survival probabilities $\Pi(t)$ and their asymptotic values Π_∞ do not allow for a clear-cut statement for the DSC. The first thing to note is that $\Pi_\infty^{(1)}$ and $\Pi_\infty^{(2)}$ are very similar and that with increasing g their values stay rather constant. This again is only a weak indication that also the DSC shows localization.

VII. SIERPINSKI CARPET

Let us now consider the transport properties of CTRW and of CTQW on SC. We start again by calculating the lower bound $|\overline{\alpha}(t)|^2$ of the quantum average return probability $\overline{\pi}(t)$, Eq. (8), see Fig. 5 for the DSC with $g = 6$. The inset shows the behavior of the corresponding CTRW $p_{1,1}(t)$ for various g, which for intermediate times scales with d_s as expected.

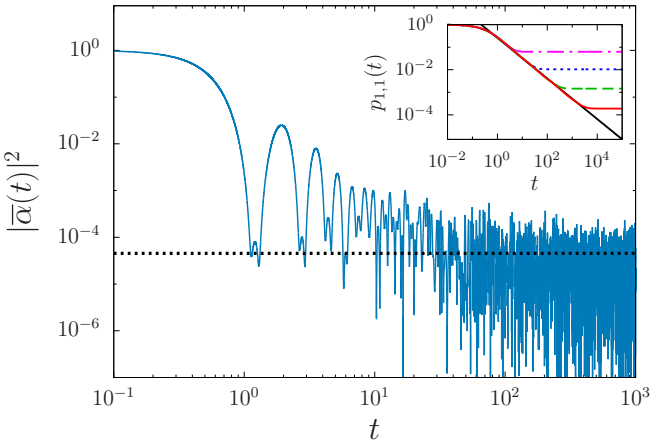

FIG. 5: (Color online) Average return amplitude on the SC at $g = 6$ (blue solid line) and the long time average $\overline{\chi}_{lb}$ (black dotted line). Inset: classical return probability to the corner node for the SC at $g = 2$, 3, 4, and 5 (pink dash dotted, blue dotted, green dashed, red solid line, respectively) and the decay according to the spectral dimension d_s (black straight solid line).

Again the finite size of the network does not allow for a definite statement about the recurrent behavior of the CTQW. Therefore, we again calculate $\rho(E)$, see Eq. (10), for the highly degenerate eigenvalue $E = 4$; the corresponding values are displayed in TABLE VII. There we also show the long time average $\overline{\chi}_{lb}$ calculated using the r.h.s. of Eq. (14). Similar to the DSC case, there is no strong evidence that CTQW on SC show localization. Again, as for DSC, the limiting value of $\rho(4)$ lies above 3×10^{-3}, such that at this point we cannot make any precise statement. We could not obtain results

g	$\rho(4)$	$\overline{\chi}_{lb}$
2	$3\,/\,16 \approx 1.88 \times 10^{-2}$	1.25×10^{-1}
3	$6\,/\,96 = 6.25 \times 10^{-2}$	1.89×10^{-2}
4	$8\,/\,688 \approx 1.16 \times 10^{-2}$	2.29×10^{-3}
5	$16\,/\,5280 \approx 3.03 \times 10^{-3}$	2.92×10^{-4}
6	$128\,/\,41584 \approx 3.08 \times 10^{-3}$	4.54×10^{-5}

TABLE VII: The $\rho(E)$ for the eigenvalue $E = 4$ and the long time average $\overline{\chi}_{lb}$ for different generations of the SC.

g	$\Pi_\infty^{(1)} = N_0^{(1)}/N$	$\Pi_\infty^{(2)} = N_0^{(2)}/N$
2	$2\,/\,16 = 0.125$	$2\,/\,16 = 0.125$
3	$23\,/\,96 \approx 0.240$	$22\,/\,96 \approx 0.230$
4	$168\,/\,688 \approx 0.244$	$168\,/\,688 \approx 0.244$
5	$1314\,/\,5280 \approx 0.249$	$1314\,/\,5280 \approx 0.249$

TABLE VIII: The asymptotic limit Π_∞ of $\Pi(t)$ for SC of generations $g = 2, 3, 4$, and 5; case (1): the traps are placed on the corner nodes, diamonds in Fig. 1(c); case (2): the traps are placed on the central nodes, squares in Fig. 1(c), see text for details.

for larger generations because (at present) we do not have the computational facilities to calculate $\rho(4)$ for $g > 7$; the size of the corresponding matrix for a DSC of $g = 7$ is already larger than $300\,000 \times 300\,000$.

Considering now absorption processes, when there are traps placed on three nodes of each network (see, e.g., Fig. 1(c)), we again calculate the quantum mechanical limit Π_∞ of $\Pi(t)$; the corresponding results are given in TABLE VIII. Here we find that CTQW on SC are quite different from those on the gaskets, but that they are similar to CTQW on DSC: both, $\Pi_\infty^{(1)}$ and $\Pi_\infty^{(2)}$, show a slow increase with increasing g.

VIII. SUMMARY

Our analysis of CTQW over different types of Sierpinski fractals revealed interesting aspects of quantum mechanical transport. At first, for SG and for DSG we find strong localization effects, supported by the fact that the long time averages $\overline{\chi}_{lb}$ approach a finite limiting value with increasing g, see TABLES I and III. For the carpets we cannot make a definite statement based on our numerical results for $\overline{\chi}_{lb}$ for generations up to $g = 6$.

Turning now to the DOS and monitoring in each case the eigenvalues with the highest degeneracy, we find that $\rho(3)$ and $\rho(5)$ for DSG and $\rho(6)$ for SG tend with growing g each to a constant, quite significant value, see TABLES I and III. This supports our view that the walkers are localized even for very large g, in line with Refs. [13, 15]. For the carpets, for which the eigenvalue with the highest degeneracy is 3 for DSC and 4 for SC, we find that the corresponding values $\rho(3)$ for the DSC and $\rho(4)$ for the SC are rather small, which renders a clear cut

decision on localization difficult. We hence conclude that one needs much larger carpets than the ones we could (at present) numerically handle, in order to attain a definite conclusion.

These results are confirmed by our findings for the mean survival probabilities $\Pi_\infty^{(j)}$ $(j = 1, 2)$ for both arrangements of traps. Here, the mean survival probability for SG and DSG increases with N, meaning that for larger networks it becomes less and less probable that the excitation will leave the network. Since in each case we consider only three trap nodes, with increasing g the number of nodes without traps increases. Hence, due to localization, an excitation starting from a node far away from the traps will not be able to reach them. For SC and DSC, the mean survival probabilities show only a slight increase with g (for the network sizes considered here), thus the probability of being trapped is almost independent of the size of the network, see TABLES VI and VIII. In this respect, it would be also interesting to investigate the effect when the number of traps also increases with g.

In addition and in contrast to the corresponding classical CTRW, for CTQW there is no apparent scaling behavior with the spectral dimension d_s. This is obvious for the gaskets, see Ref. [6] for DSG and Fig. 3 for SG. However, for the carpets one might still argue that for large generations g such a scaling could exist for the envelope of $|\overline{\alpha}(t)|^2$ at intermediate times, see Figs. 4 and 5. But from our numerical results for generations up to $g = 7$ we cannot draw this conclusion.

Nevertheless, the long time behavior of the CTQW with and without traps reveals clear-cut differences between gaskets and carpets for the generations studied here. While classically the difference is only manifested in a different scaling according to d_s, quantum-mechanically we find there appears to be a fundamental difference between gaskets and carpets - at least for the finite networks studied here. Our main results are summarized in Fig. 6, where we plot, as a function of the number of nodes N, the long time average of the lower bound of the averaged return probability, $\overline{\chi}_{lb}$, and (for practical purposes) the long time value of the mean trapping probability, i.e., $1 - \Pi_\infty^{(j)}$ $(j = 1, 2)$, for the two situations of trap arrangements.

Already the spectra of the gaskets and of the carpets are significantly different and contain - in principle - all the essential information. Now, for the classical CTRW only the low-energy part of the spectrum is important for the intermediate-to-long time behavior, whereas for CTQW the whole spectrum matters. Clearly, further investigations of these facts are in order, but go beyond the scope of the present paper. In general, a systematic study of the importance of the so-called ramification number (the number of nodes/bonds which has to be removed in order for the fractal to fall apart), along with a careful analysis of localized eigenstates (e.g., "dark states" for the trap) deserves further studies. From the point of view of bond percolation, we have studied localized eigenstates of two dimensional lattices with traps and with randomly placed bonds [46]. There, we found that the localization feature is also mirrored in the survival probablity. While these aspects have been already touched upon in Ref. [21] for the SG, no detailed analysis has been carried out for the SC.

ACKNOWLEDGMENTS

We thank Dr. János Asbóth for stimulating discussions. We further thank the Deutscher Akademischer Austauschdienst (DAAD Grant No. 56266206 and project no. 40018) for supporting mutual visits of the Freiburg and the Budapest groups. Z.D. and T.K. acknowledge support by the Hungarian Scientific Research Fund (OTKA) under contract nos. K83858 and NN109651, and the Hungarian Academy of Sciences (Lendület Program, LP2011-016). A.A., A.B., and O.M. acknowledge support from the Deutsche Forschungsgemeinschaft (DFG Grant No. MU2925/1-1), from the Fonds der Chemischen Industrie, and from the Marie Curie International Research Staff Exchange Science Fellowship within the 7th European Community Framework Program SPIDER (Grant No. PIRSES-GA-2011-295302).

[1] S. Havlin and R. Cohen, *Complex Networks: Structure, Robustness and Function* (Cambridge University Press, 2010).
[2] R. Albert and A.-L. Barabási, Rev. Mod. Phys. **74**, 47 (2002).
[3] M. Doi and S. F. Edwards, *The Theory of Polymer Dynamics* (Oxford University Press, Oxford, 1988).
[4] R. Albert, I. Albert, and G. L. Nakarado, Phys. Rev. E **69**, 025103 (2004).
[5] B. Yu and M. P. Singh, in *Proceedings of the Second International Joint Conference on Autonomous Agents and Multiagent Systems*, AAMAS '03 (ACM, 2003) pp. 65–72.
[6] E. Agliari, A. Blumen, and O. Mülken, J. Phys. A: Math. Theor. **41**, 445301 (2008).
[7] A. Blumen and A. Jurjiu, J. Chem. Phys. **116**, 2636 (2002).
[8] M. G. Cosenza and R. Kapral, Phys. Rev. A **46**, 1850 (1992).
[9] N. Van Kampen, *Stochastic Processes in Physics and Chemistry*, North-Holland Personal Library (Elsevier Science, 2011).
[10] G. H. Weiss, *Aspects and applications of the random walk*, Random Materials and Processes Series (North-Holland, 1994).
[11] G. Pólya, Mathematische Annalen **84**, 149 (1921).
[12] S. Condamin, O. Bénichou, V. Tejedor, R. Voituriez, and J. Klafter, Nature **450**, 77 (2007).
[13] O. Mülken and A. Blumen, Phys. Rep. **502**, 37 (2011).
[14] S. Alexander, J. Bernasconi, W. R. Schneider, and R. Orbach, Rev. Mod. Phys. **53**, 175 (1981).
[15] O. Mülken and A. Blumen, Phys. Rev. E **73**, 066117 (2006).
[16] A. Anishchenko, A. Blumen, and O. Mülken, Quant. Inf. Proc. **11**, 1273 (2012).
[17] O. Mülken, V. Bierbaum, and A. Blumen, J. Chem. Phys. **124**, 124905 (2006).
[18] S. E. Venegas-Andraca, Quant. Inf. Proc. **11**, 1015 (2012).
[19] E. Agliari, A. Blumen, and O. Mülken, Phys. Rev. A **82**, 012305 (2010).

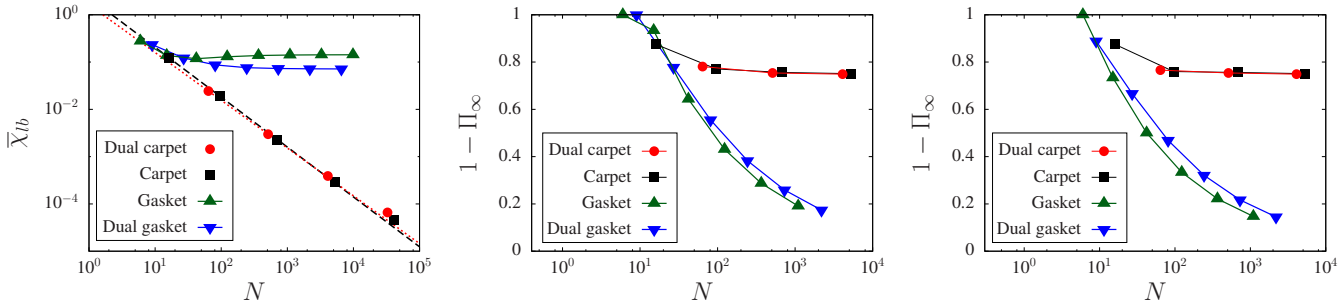

FIG. 6: (Color online) Long time average $\overline{\chi}_{lb}$ of $\pi_{1,1}(t)$ and probability $1-\Pi_\infty$ for an excitation to get trapped as a function of the number of nodes.

[20] A. Patel and K. S. Raghunathan, Phys. Rev. A **86**, 012332 (2012).
[21] E. Domany, S. Alexander, D. Bensimon, and L. P. Kadanoff, Phys. Rev. B **28**, 3110 (1983).
[22] X. R. Wang, Phys. Rev. B **51**, 9310 (1995).
[23] M. Li, Y. Liu, and Z.-Q. Zhang, Phys. Rev. B **61**, 16193 (2000).
[24] M. C. Rechtsman, J. M. Zeuner, Y. Plotnik, Y. Lumer, D. Podolsky, F. Dreisow, S. Nolte, M. Segev, and A. Szameit, Nature **496**, 196 (2013).
[25] A. Schreiber, A. Gábris, P. P. Rohde, K. Laiho, M. Štefaňák, V. Potoček, C. Hamilton, I. Jex, and C. Silberhorn, Science **336**, 55 (2012).
[26] E. Farhi and S. Gutmann, Phys. Rev. A **58**, 915 (1998).
[27] M. Štefaňák, B. Kollár, T. Kiss, and I. Jex, Phys. Scr. **2010**, 014035 (2010).
[28] B. Kollár, M. Štefaňák, T. Kiss, and I. Jex, Phys. Rev. A **82**, 012303 (2010).
[29] M. Štefaňák, I. Jex, and T. Kiss, Phys. Rev. Lett. **100**, 020501 (2008).
[30] M. Štefaňák, T. Kiss, and I. Jex, New J. Phys. **11**, 043027 (2009).
[31] X.-K. Zhang, J. Wan, J.-J. Lu, and X.-P. Xu, Commun. Theor. Phys. **56**, 293 (2011).
[32] J. Wan and X.-P. Xu, Physica A **391**, 1919 (2012).
[33] F. A. Grünbaum, L. Velázquez, A. H. Werner, and R. F. Werner, Commun. Math. Phys. **320**, 543 (2013).
[34] Z. Darázs and T. Kiss, Phys. Rev. A **81**, 062319 (2010).
[35] R. Rammal and G. Toulouse, J. Phys. Lett. (Paris) **44**, 13 (1983).
[36] M. T. Barlow and R. F. Bass, Proc. R. Soc. Lond. A **431**, 345 (1990).
[37] O. Mülken, arXiv preprint arXiv:0710.3453 (2007).
[38] O. Mülken, A. Blumen, T. Amthor, C. Giese, M. Reetz-Lamour, and M. Weidemüller, Phys. Rev. Lett. **99**, 090601 (2007).
[39] M. Gönülol, E. Aydıner, Y. Shikano, and O. E. Müstecaplıoğlu, New J. Phys. **13**, 033037 (2011).
[40] P. Schijven, J. Kohlberger, A. Blumen, and O. Mülken, J. Phys. A: Math. Theor. **45**, 215003 (2012).
[41] O. Mülken, V. Pernice, and A. Blumen, Phys. Rev. E **78**, 021115 (2008).
[42] S. Alexander and R. Orbach, J. Phys. Lett. (Paris) **43**, 625 (1982).
[43] H. Fang and Y. Saad, *A filtered Lanczos procedure for extreme and interior eigenvalue problems*, Tech. Rep. Report umsi-2011-xx (Minnesota Supercomputer Institute, University of Minnesota, 2011).
[44] S. M. Heilman and R. S. Strichartz, Fractals **18**, 1 (2010).
[45] M. Begue, T. Kalloniatis, and R. S. Strichartz, Fractals **21**, 1350002 (2013).
[46] A. Anishchenko, A. Blumen, and O. Mülken, Phys. Rev. E **88**, 062126 (2013).